

Investigation of the Effect of Different Factors on the Performance of Several Perovskite Solar Cells: A Simulation Study by SCAPS

Hasan MallaHasan^{1,2}, and Özlem Onay^{3*}

- ¹ Aleppo University, Mechanical Power Engineering, Aleppo, Syria
- ² Eskişehir Technical University, Graduate Education Institute, Eskişehir, Turkey
- ³ Prof, Eskişehir Technical University, Porsuk Vocational School, Eskisehir, Turkey

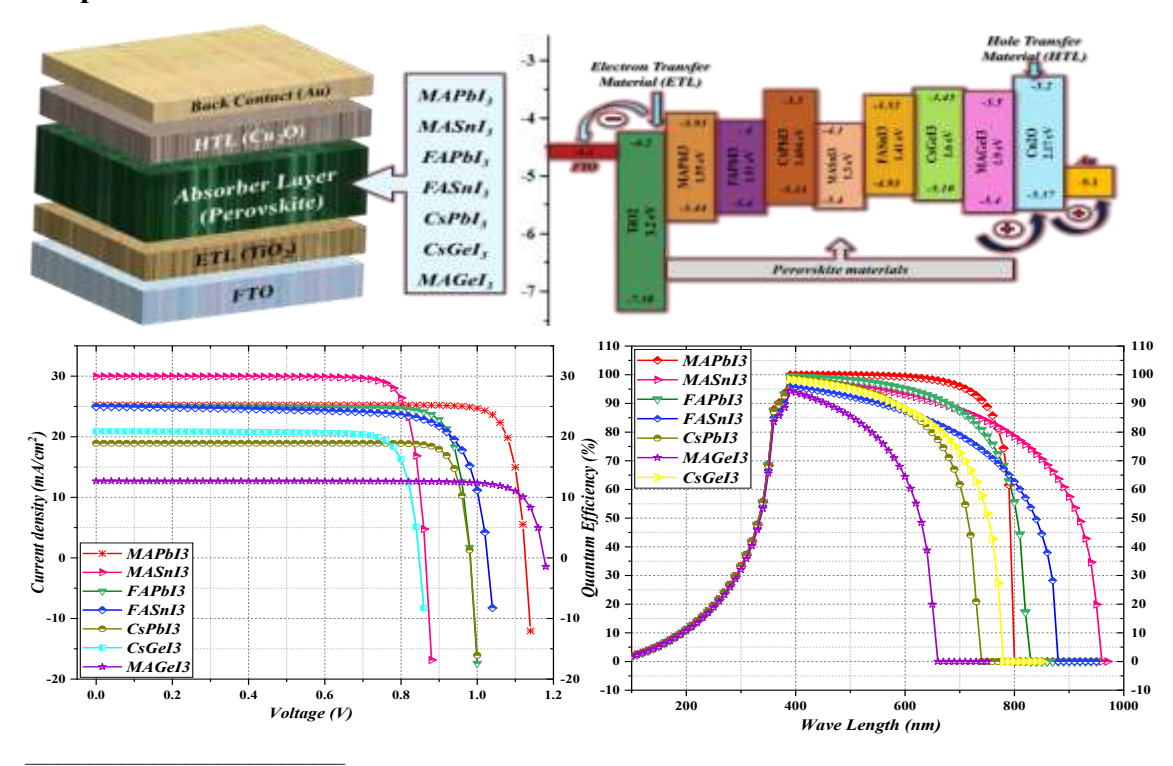
ARTICLE INFO

ABSTRACT

Kevwords:

Perovskite solar cells, Lead-based perovskite, Lead-free perovskite, SCAPS-1D The new generation of solar cells based on perovskite materials has attracted massive attention from the photovoltaic community, due to their high capability in supporting low-cost solar cell. In this study, extensive theoretical research of three types of lead-based (MAPbI₃, FAPbI₃ and CsPbI₃) and four types of lead-free (MASnI₃, FASnI₃, CsGeI₃, and MAGeI₃) perovskite solar cells are modeled while Cu₂O is used as HTL and TiO₂ as ETL. The initial results show commendable performance for MAPbI₃ with 24,8% efficiency, while MAGeI₃ has the lowest performance (12,61%). In addition, different factors reviewed affect the performance almost similarly to the studied types of perovskites.

Graphical abstract



^{*} Corresponding Author E-Mail Address: oonay@eskisehir.edu.tr

Cite this article as:

MallaHasan, H., & Onay, O. (2022). Investigation of the Effect of Different Factors on the Performance of Several Perovskite Solar Cells: A Simulation Study By SCAPS. European Journal of Engineering Science and Technology, 5(1): 20-38. https://doi.org/10.33422/ejest.v5i1.927

© The Author(s). 2022 **Open Access**. This article is distributed under the terms of the <u>Creative Commons Attribution 4.0 International License</u>, which permits unrestricted use, distribution, and redistribution in any medium, provided that the original author(s) and source are credited.



1. Introduction

The significant growth of Perovskite Solar Cells (PSCs) in the recent decade and their outstanding electrical and optical properties including appropriate and tunable band-gap, high absorption coefficient and low exciton-binding energy, as well as low-cost processing, attract the attention of researchers around the world (Jayan K et al., 2021; Raj et al., 2021). In just a short period, the perovskite photovoltaics, especially the lead-based types, achieved very high Power Conversion Efficiency (PCE) of 25.7% compared with other one junction solar cell technologies, and consequently emerged as a suitable contender in the future photovoltaic market (NREL, 2022; Tang et al., 2017). However, the environmental concerns about leadbased perovskites due to the high toxicity of lead, besides the instability of PSCs in ambient environment, impedes the procedure of commercialization (Tonui et al., 2018). Therefore, it is important to look for the metal elements that have similar electronic characteristics like Pb to be able to produce a stable nontoxic perovskite solar cell. A number of publications have mentioned this issue by substituting Sn and Ge instead of Pb in perovskite structures as an absorbing layer. This replacement solves the instability against moisture and toxicity problem; however, it also limits the device performance significantly (Kumar et al., 2020). In addition, the use of formamidinium (FA)1 instead of methylammonium (MA)2 in perovskite structure has improved the problem of moisture instability, though the reason this type is not suitable in the long run is that FAPbI₃ suffers from two different phases at room temperature. On the other hand, another way which been addressed in literature to improve the instability issues of perovskite is the incorporation of inorganic cesium (Cs) into perovskite compositions with MA and FA. This new class of perovskite material has attracted great interest from researchers to investigate its additional properties and enhance the performance of PSCs along with stability. (Raza et al., 2021).

In this work, a comparative simulation study was carried out for three lead-based MAPbI₃, FAPbI₃ and CsPbI₃ and four lead-free MASnI₃, FASnI₃, CsGeI₃, and MAGeI₃ as absorbing material in PSC while Cu₂O and TiO₂ were used as Hole Transfer Layer (HTL) and Electron Transfer Layer (ETL), respectively. The aim of this study is to investigate the effect of different factors on the PSC performance and therefore optimize the devices depending on the simulation results. The effect of the thickness of the absorber layer, defect density, the ambient temperature, the parasitic resistances including series and shunt resistances, the back contact metal and CBO and VBO on the PSC performance have been presented.

2. Methodology

2.1. SCAPS and simulation authenticating

This study was carried out with one dimensional Solar Cell Capacity Simulator (SCAPS-1D) software for numerical modeling of perovskite solar cells. The simulation methodology of SCAPS-1D is based on solving equations controlling semiconductor materials for electron/hole carriers, these are, the carrier-continuity equation, Poisson's equation, and the drift diffusion equation (Burgelman et al., 2000, 2021; Lenka et al., 2020). Numerical simulation facilitates the understanding of the basics of solar cells and helps to determine the major characteristics that affect their performance. The Poisson equation represents the relationship between the electric field of a p-n junction (E) and the space charge density (ρ) (Minemoto & Murata, 2014; Nalianya et al., 2021), given as follows:

¹ (MA): Methylammonium = $CH_3NH_3^+$

² (**FA**): Formamidinium = $CH_2(NH_2)_2^+$

$$\frac{\partial^2 \psi}{\partial x^2} = -\frac{\partial E}{\partial x} = -\frac{\rho}{\varepsilon_s} = -\frac{q}{\varepsilon_s} \left[p - n + N_D^+(x) - N_A^-(x) \pm N_{def}(x) \right] \tag{1}$$

 ψ : the electrostatic potential p (n) : the hole (electron) density

q: elementary charge $N_A^-(N_D^+)$: the density of ionized acceptors (donors)

static relative permittivity of the N_{def} : the defect density (Donor or acceptor)

The electron and hole continuity equations in steady state are given by:

$$-\frac{\partial j_n}{\partial x} - U_n + G = \frac{\partial n}{\partial t} \\
-\frac{\partial j_P}{\partial x} - U_P + G = \frac{\partial p}{\partial t}$$
(2)

Where: j_n, j_p are the electron and hole current densities; $U_{n,p}$ is the net recombination rates; G is the electron-hole generation rate.

The electron and hole current density are given by:

$$J_{n} = -\frac{\mu_{n}n}{q} \frac{\partial E_{F_{n}}}{\partial x}$$

$$J_{P} = +\frac{\mu_{n}P}{q} \frac{\partial E_{F_{p}}}{\partial x}$$

$$(3)$$

q is the elementary charge, $\mu_{n(p)}$ is electron (hole) mobility, and $D_{n(p)}$ is the diffusion coefficient of electrons (holes).

Many published work in the literature such as (Houimi et al., 2021; Karimi & Ghorashi, 2017; Karthick et al., 2020) confirm that data obtained from SCAPS software correspond highly to real results, especially when parasitic resistances and defects are taken into account. Thus, it authenticates the simulation results in this study and renders them reliable.

2.2. Layers parameters and devices configuration

The parameters of perovskite materials are extracted from literature (Abdelaziz et al., 2020; Abnavi et al., 2021; Chen et al., 2016; Deepthi Jayan & Sebastian, 2021; Gélvez-Rueda et al., 2017; Kanoun et al., 2019; Karimi & Ghorashi, 2017; Karthick et al., 2020; Kumar et al., 2020; Patel, 2021; Raj et al., 2021; Sarker et al., 2021; A. K. Singh et al., 2021; Tao et al., 2019; Tara et al., 2021; Zhao et al., 2017) and listed in Table 1, and the parameters of FTO, ETL and HTL are listed in Table 2, while the defect density values at interfaces are listed in Table 3. The simulation was carried out under sunlight and the device illuminated from the ETL side by the AM1.5G spectrum (1000 W.m⁻²), and the ambient temperature was assumed to be 300 K. The PSC devices configuration and the energy levels for all used materials has been shown in Figure 1 and Figure 2. respectively.

Table 1. *Physical parameters of the PSC used for this simulation study*

Material property	$MAPbI_3$	MASnI ₃	$FAPbI_3$	FASnI ₃	$CsPbI_3$	MAGeI3	$CsGeI_3$
Thickness, t (nm)	850	450	350	350	450	350	400
Bandgap, E_g (eV)	1.55	1.3	1.51	1.41	1.694	1.9	1.6
Electron affinity, X	3.9	4.2	4.0	3.9	3.95	3.98	3.523
(eV)	2.0	0.0		0.0		1.0	10
Relative dielectric permittivity ε_r	30	8.2	6.6	8.2	6	10	18
Conduction band effective density of states N_C (1/cm ³)	2×10^{18}	1×10^{18}	1.2×10^{19}	1.0×10^{18}	1.1×10^{20}	1×10^{16}	1.0×10^{18}
Valence band effective density of states N _V (1/cm ³)	2×10^{19}	1×10^{18}	2.9×10^{18}	1.0×10^{18}	8×10^{19}	1 ×10 ¹⁵	1.0× 10 ¹⁹
Electron mobility, μ_n (cm ² /Vs)	10	1.6	2.7	22	25	16.2	20
Hole mobility, μ _h (cm ² /Vs)	10	1.6	1.8	22	25	10. 1	20
Donor	_	$1 \times 10^{14*}$	1.3×10^{16}	_	1×10^{15}	1×10^{9}	_
density, N _D (1/cm ³)							
Acceptor density,	1.0×	_	1.3×10^{16}	7.0×10^{16}	_	1×10^{9}	2×10^{16}
$N_A (1/cm^3)$	10^{17}						
Total density (cm ⁻³)	2.0×10^{14}	5.0×10^{14}	4.0×10^{14}	2.0×10^{15}	2.07×10^{14}	1.0×10^{15}	1.0×10^{15}

Absorption interpolation model is set at 1.0×10^5 (cm⁻¹) and thermal velocity of electron and hole are set as 1.0×10^7 (cm/s) for all materials.

Table 2.

Input parameters of FTO, ETL and HTL (N. E. Courtier et al., 2019; Nicola E. Courtier et al., 2019; Karimi & Ghorashi, 2017; Raoui et al., 2019; R. Singh et al., 2019)

Material property	Cu ₂ O (HTL)	TiO ₂ (ETL)	FTO
Thickness (nm)	50*	50*	200*
Bandgap, E_g (eV)	2.17	3.2	3.5
Electron affinity (eV)	3.2	4	4
Relative dielectric permittivity, ε_r	7.1	10	9
CB effective density of states	2.5×10^{20}	5.0×10^{19}	2.2×10^{18}
$N_{\rm C}$ (1/cm ³)			
VB effective density of states N _V	2.5×10^{20}	5.0×10^{19}	1.8×10^{19}
$(1/\text{cm}^3)$			
Electron mobility, μ_n (cm ² /Vs)	200	6.0×10^{-3}	20
Hole mobility, μ_h (cm ² /Vs)	8600	6.0×10^{-3}	10
Donor density, N _D (1/cm ³)	0	1.0×10^{18}	1.0×10^{19}
Acceptor density, N _A (1/cm ³)	1×10^{18}	0	0
Total density (cm ⁻³)	1.0×10 ¹³	$1.0 \times 10^{18} / 1.0 \times 10^{17}$	1.0×10^{15}

^{*}In this study.

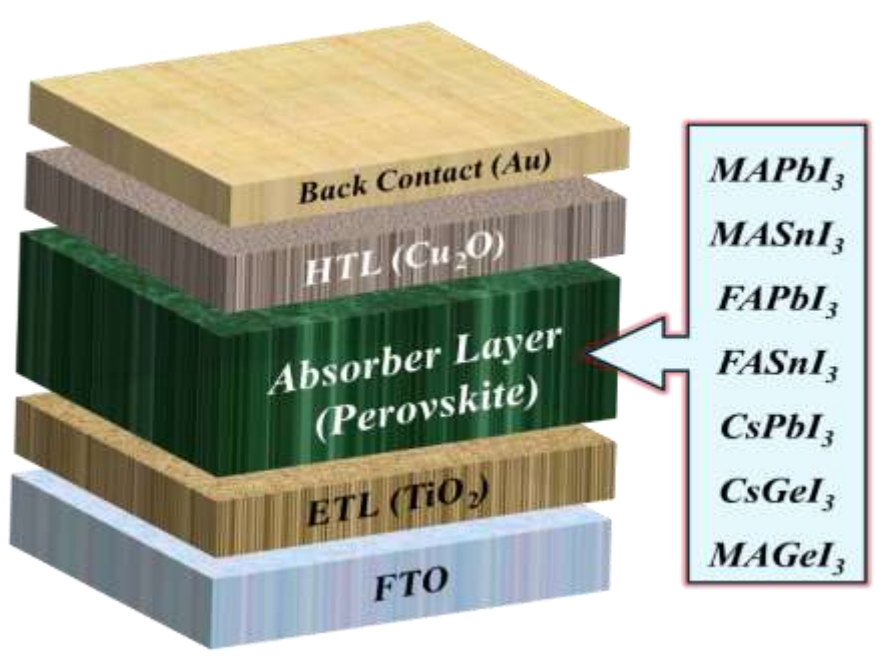


Figure 1. The architecture design of PSC devices

Table 3.

Defect density values at interfaces of all simulated devices (Abdelaziz et al., 2020; Kumar et al., 2020; Raoui et al., 2019)

Parameter Parameter	HTL/Perovskite	Perovskite/ ETL
Defect density	Donor	Acceptor
Electron capture cross section (cm ⁻²)	1×10^{-15}	1×10^{-16}
Hole capture cross section (cm ⁻²)	1×10^{-16}	1×10^{-16}
Energetic distribution	Gaussian	Gaussian
Energy level relative to E _v	0.600	0.600
Total density (cm ⁻³)	1×10^{10}	1.0×10^{10}

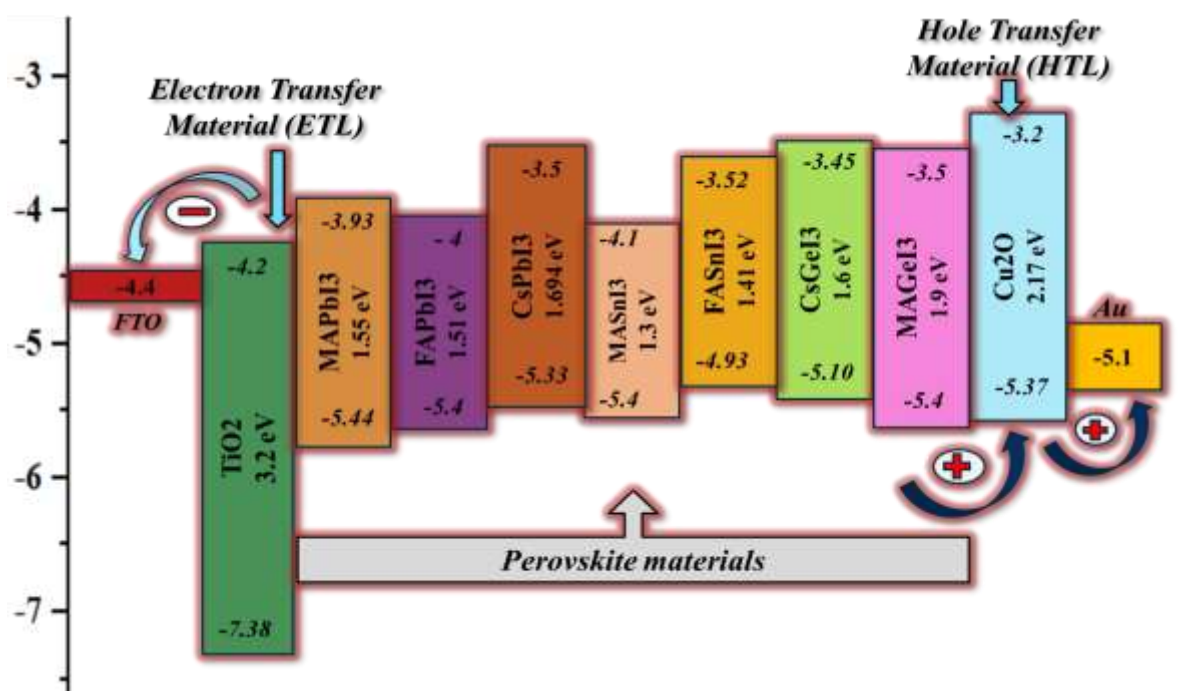


Figure 2. Energy levels for all used materials in the PSC devices

3. Results and discussion

3.1. The initial results of simulation

The simulation study is applied via SCAPS-1D program for seven types of PSCs with perovskite materials (MAPbI₃, FAPbI₃, MASnI₃, FASnI₃, CsPbI₃, CsGeI₃ and MAGeI₃) as absorber layer, Cu₂O as HTL and TiO₂ as ETL. The initial results of the simulation are listed in Table 4. Since J-V curve define the performance characteristics of solar cell, J-V curves of all devices are presented in Figure 3. As shown in the results, the most efficient device is the MAPbI₃ with PCE up to (24.8%), but the MASnI₃-based device has the highest value of short circuit current (29.96 mA/cm²) and MAGeI₃ has the lowest (12.67 mA/cm²). However, MAGeI₃ shows higher open circuit voltage (1.176 V) compared with other types, while CsGeI₃ record the minimum V_{OC} value between all devices (0.849 V).

Table 4.

Summary of the initial results of PSCs performance parameters extracted from the simulation with (FTO/TiO₂/Perovskite materials/Cu₂O/Au) device configuration

Perovskites	Open Circuit Voltage (V _{OC})	Short Circuit Current Density	Fill Factor (FF) (%)	Power Conversion Efficiency PCE
	(Volt)	(J_{SC}) (mA.cm ⁻²)	(11) (70)	(%)
MAPbI ₃	1.127	25.25	87.13	24.8
MASnI ₃	0.865	29.96	84.62	21.94
FAPbI ₃	0.982	24.93	85	20.82
FASnI ₃	1.028	24.96	76.73	19.69
CsPbI ₃	0.982	18.92	87.38	16.23
CsGeI ₃	0.849	20.89	83.39	14.78
MAGeI ₃	1.176	12.67	84.59	12.61

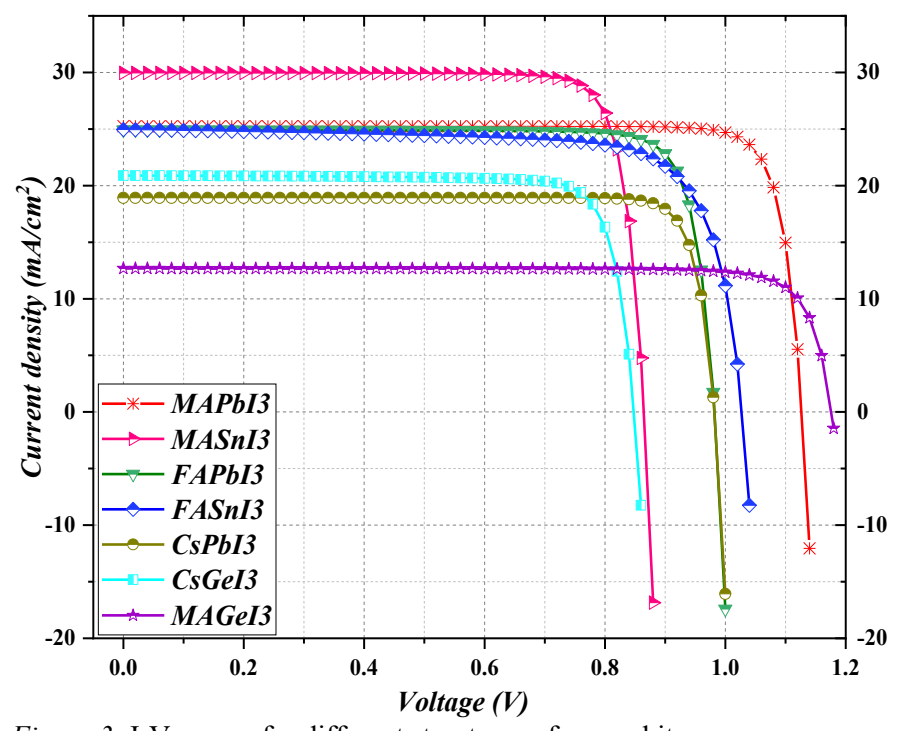


Figure 3. J-V curves for different structures of perovskites

Another defining feature of solar cells' performance is the quantum efficiency (QE) curve which facilitates understanding of the solar cell spectral response. Quantum efficiency curves for all simulated devices are shown in Figure 4.

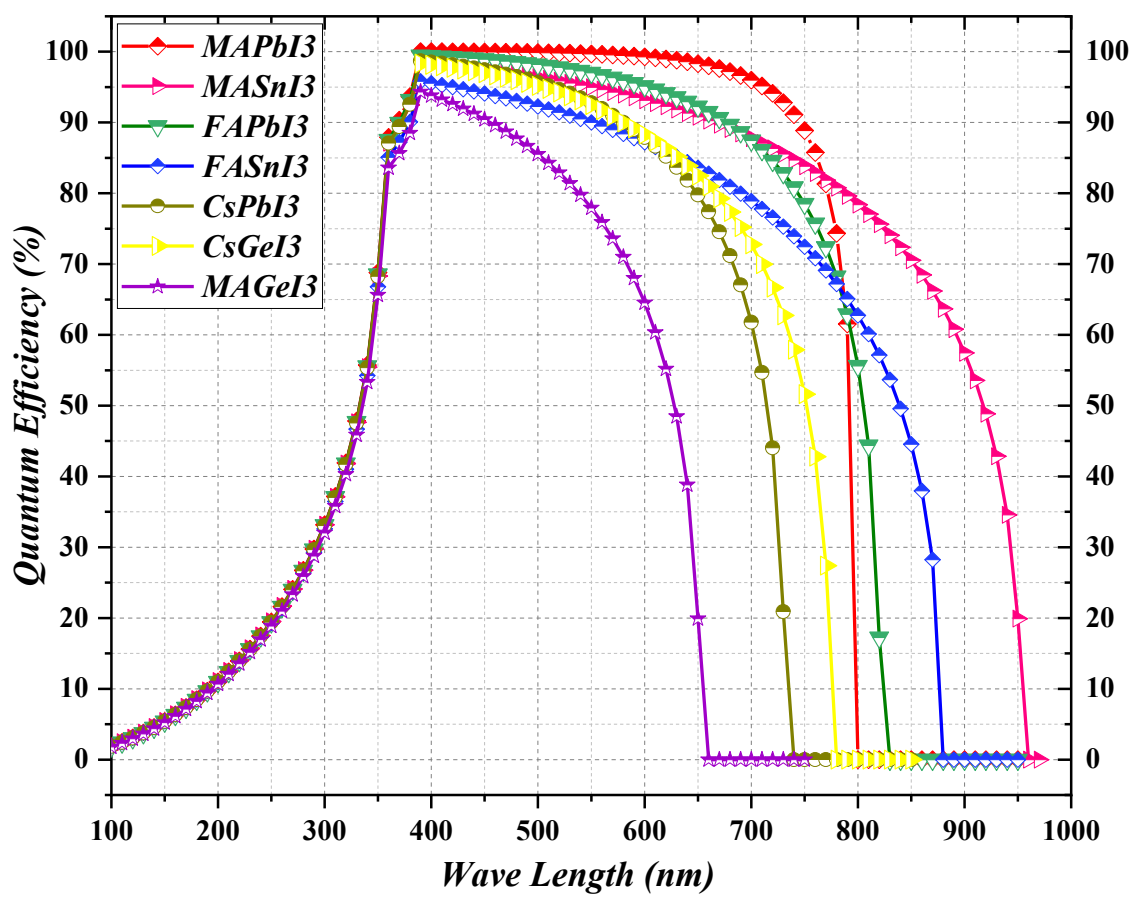


Figure 4. Quantum efficiency curves for different structures of perovskites

It can be concluded from the figure that all devices show a similar behavior of absorbing about 2% of the solar spectrum at 100 nm wave length and increase rapidly to approximately 100% at 390 nm, subsequently it starts to decrease gradually until they drop instantly to nearly zero at different wave lengths (MAPbI₃, FAPbI₃, MASnI₃, FASnI₃, CsPbI₃, CsGeI₃ and MAGeI₃ at 800 nm, 960 nm, 830 nm, 880 nm, 740 nm, 780 nm and 660 nm, respectively). This variation in spectral response of devices can be attributed to the differences in band gap values of the absorber layer. Therefore, the relatively narrow band gap of MASnI₃ (1.3 eV) enables it to absorb the spectrum up to 960 nm, while the high band gap value for MAGeI₃ (1.9 eV) limits the absorption after 660 nm of spectrum wave length (Abnavi et al., 2021).

3.2. The effect of thickness of the absorber layer

To analayse the impact of absorber layer thickness on the PSC performance, the simulation was done with absorber layer thicknesses ranging between 200 nm and 2000 nm for the seven studied types of PSCs. The optimum performance for MAPbI₃, FAPbI₃, MASnI₃, FASnI₃, CsPbI₃, CsGeI₃ and MAGeI₃ is obtained at 1200 nm, 650 nm, 750 nm, 500 nm, 2000 nm, 750 nm ve 850 nm respectivly. The simulation results of PSCs performance parameters are presented in Figure 5. The effects of photon absorption rate and charge carrier recombination are the major reasons for the loss in efficiency on both sides of the optimal thickness of the absorber (Deepthi Jayan & Sebastian, 2021). By increasing absorber layer thickness, it absorbs a bigger quantity of photons; however, the recombination rate also increases simultaneously. Therefore any more increments of the absorber thickness above the optimum value impact the performance negatively.

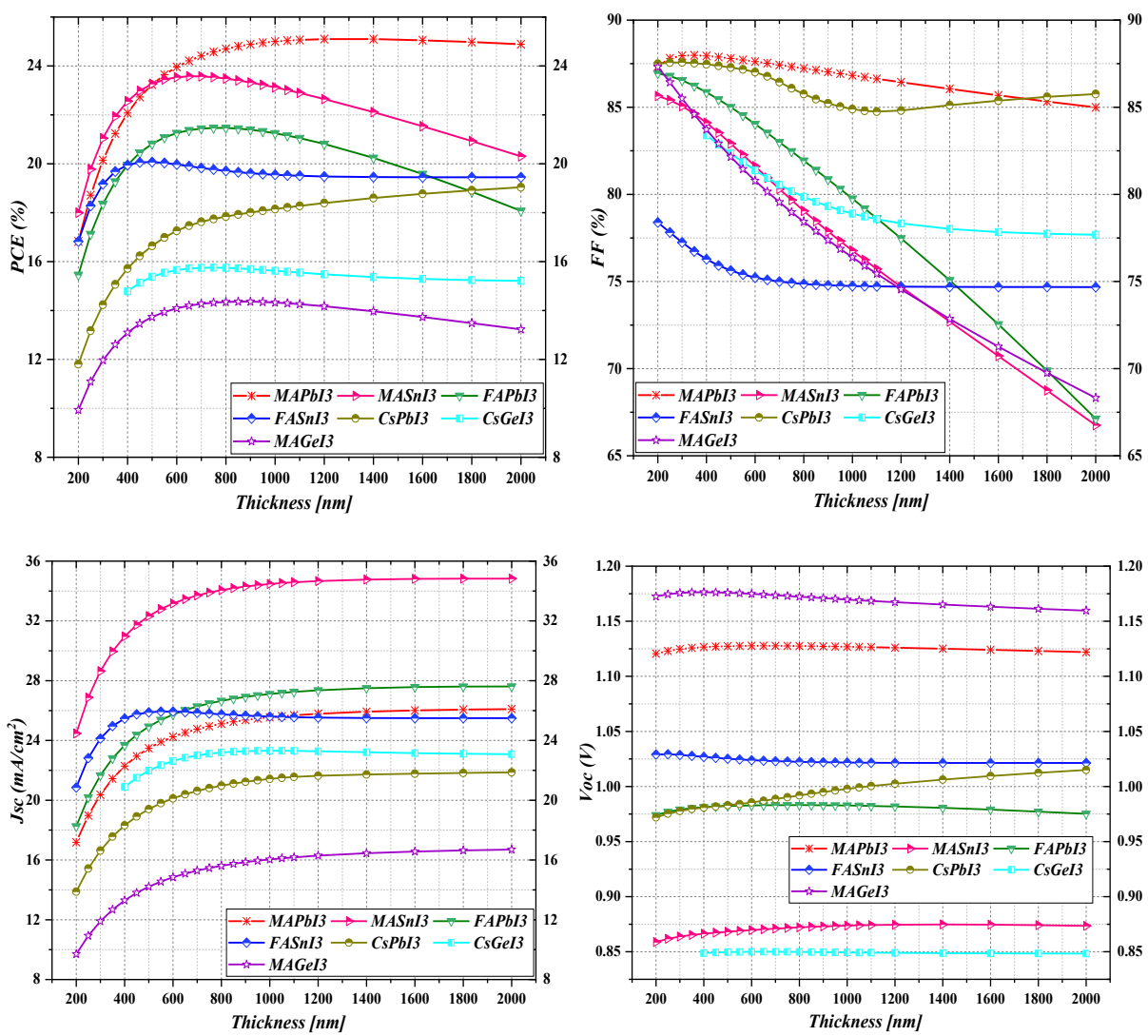


Figure 5. The effect of absorber layer thickness on PSCs performance parameters (a)PCE (b) FF. (c) $J_{SC}(d) V_{OC}$

On the other hand, decreasing the thickness under the optimum value for each device configuration also decreases the efficiency of PSCs. The reason for this is the fact that a lesser number of photons are absorbed when the active layer is too thin. Consequently, it is significant to attain an optimum value of absorber thickness which achieves an accurate balance between carrier transport and illumination absorption in order to obtain better performance of PSCs (Deepthi Jayan & Sebastian, 2021; Liu et al., 2014).

3.3. The effect of the absorber defect density

In PSC devices, high defect densities in the material of absorbent layer degrade the quality of the material and facilitate carrier recombination. Thus, the defects negatively impact the performance parameters of solar cells (Kanoun et al., 2019). To investigate and demonstrate the effect of the absorption layer defect density on the properties of PSC devices, simulation of the performance of the seven selected devices wa carried out. The simulation was performed by changing the defect density from (1×10^{13}) to (1×10^{16}) cm⁻³ and results plotted in Figure 6. As can be noticed from the figure, the efficiency reduced dramatically for each device when the defect density was as high as 1×10^{16} cm⁻³ (as it shown in a Table 5.). This might be associated to the increase of resistances. (Kanoun et al., 2019).

Table 5. Comparison of the efficiency of perovskites when changing the defect density from (1×10^{13}) cm⁻³ to (1×10^{16}) cm⁻³

	MAPbI ₃	MASnI ₃	FAPbI ₃	FASnI ₃	CsPbI ₃	CsGeI ₃	MAGeI ₃
$N_t(1/cm^3)$	PCE (%)						
1×10^{13}	25.36	22.37	21.49	20.49	16.30	15.20	13.37
1×10^{16}	20.26	17.36	15.34	12.28	14.60	12.45	10.56

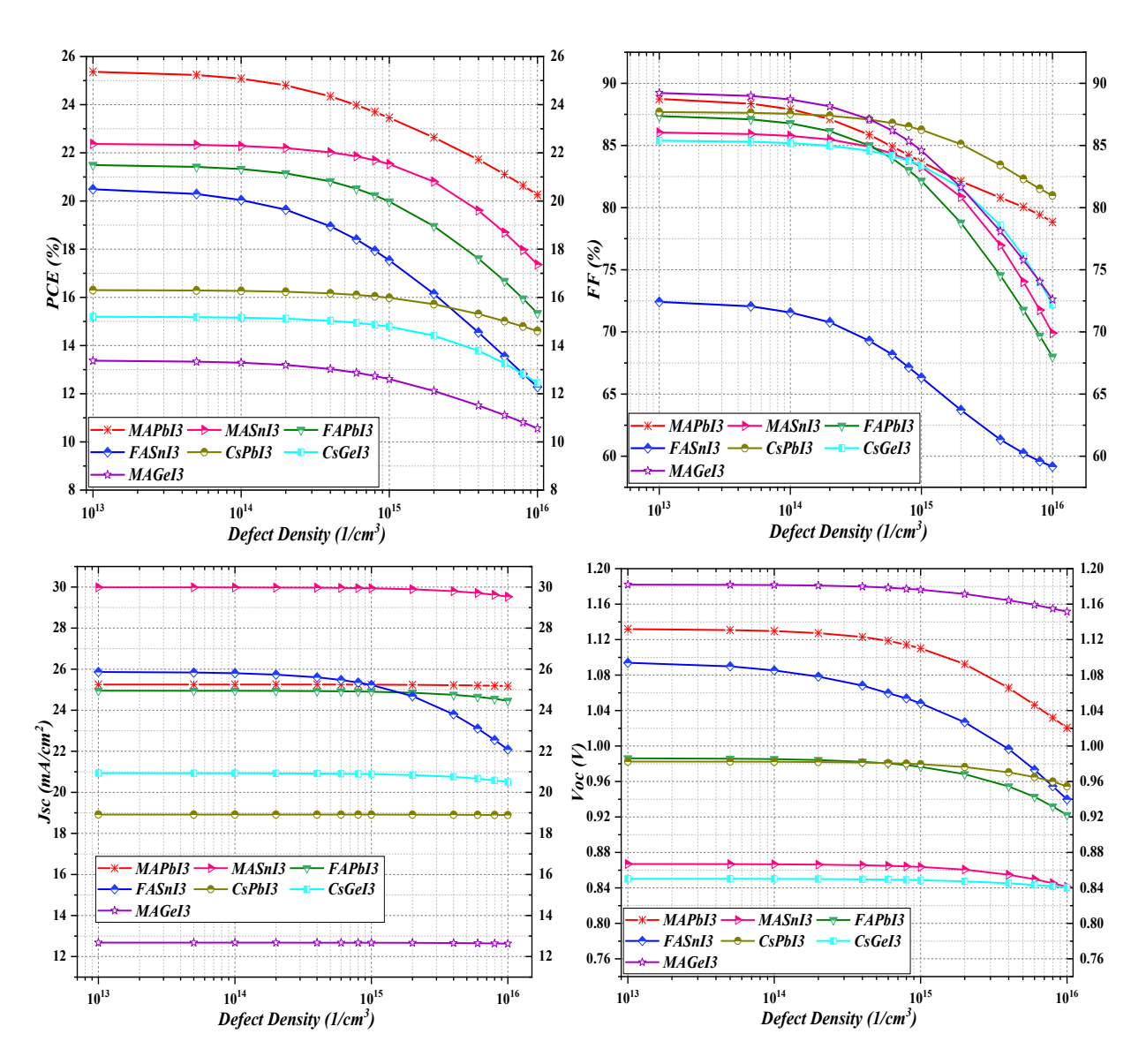


Figure 6. The effect of defect density of absorber layer on PSCs performance characteristics

3.4. The temperature effect on PSCs performance

The operating temperature of the device strongly influences the performance characteristics of PSCs. Once the PSCs are exposed to outdoor applications, the device performance is greatly affected by the atmospheric temperature (Kumar et al., 2022). The ambient temperature of the simulated device was set to be 300 K in the previous and later sections of the study. To realize the effect of temperature on device performance, simulations were done for all studied devices with changing temperature between 260 K and 400 K. Figure 7 illustrates the variation of PSCs performance parameters with operating temperature for all seven studied perovskite layers.

All simulated devices' results exhibit similar behavior: when the temperature increases, the PSC performance parameters decrease, except for the short circuit current which is almost not or very slightly influenced. This can be explained by the fact that defect density inside the layers increases with the temperature and thus reduces the efficiency (Slami et al., 2020). The reduction of PSC efficiency with temperature increment can also be attributed to the fact that several physical characteristics of PSC, such as band gap, carrier concentration and electron and hole mobility, are also affected by the operating temperature (Chakraborty et al., 2019; Kumar et al., 2022).

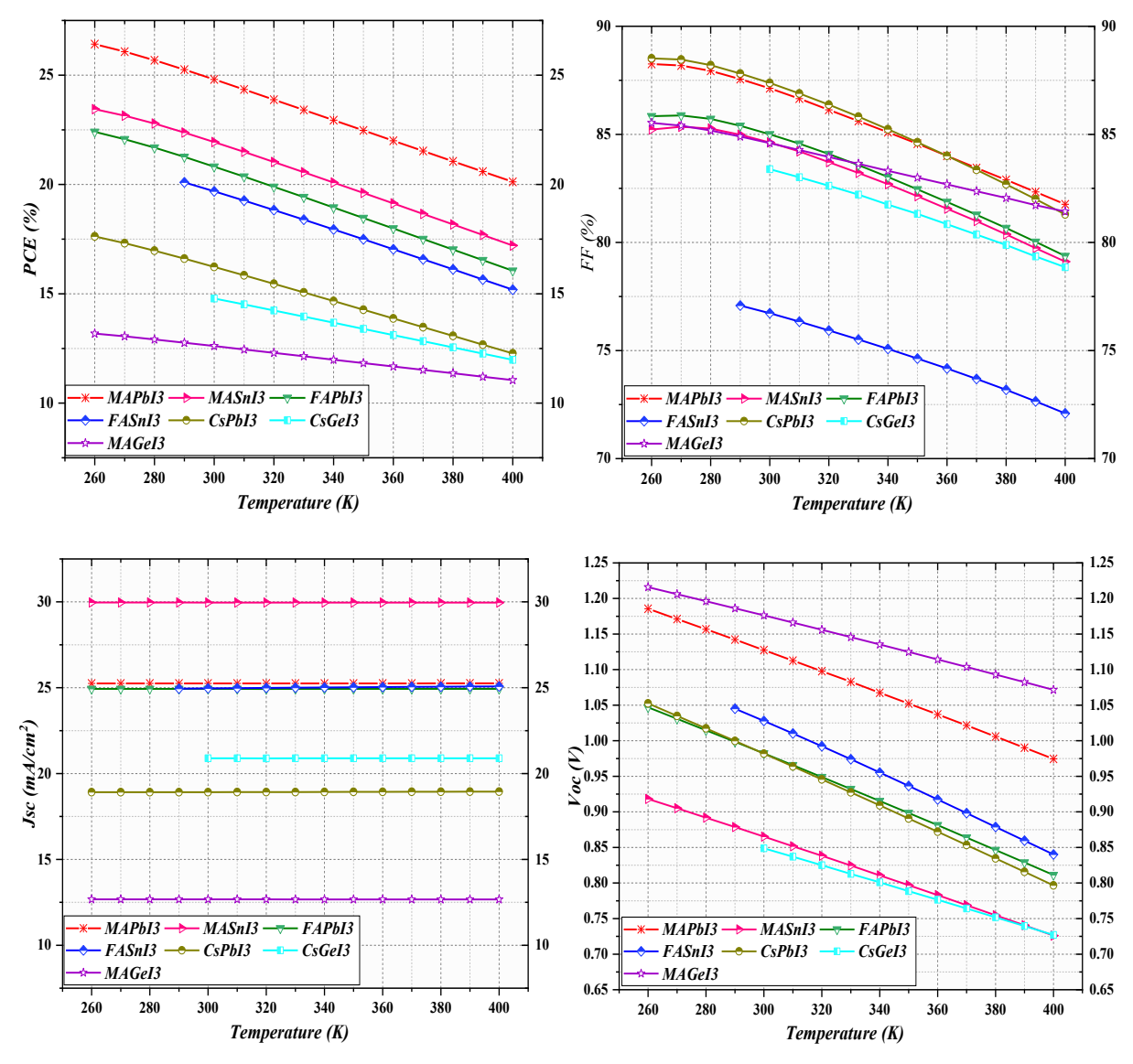


Figure 7. The effect of operating temperature on perovskite solar cells performance (a) PCE (b) FF (c) J_{SC} (d) V_{OC}

3.5. The parasitic resistances

Both shunt and series resistances have a critical impact on device performance because they control the slopes and shape of the Current – Voltage characteristics (Karthick et al., 2020). The parasitic resistances could result from the defects produced by the material itself and during manufacturing procedure, as well as the back contact. In a standard diode model, the J–V characteristic of a heterojunction solar cell are given by equation (4) (Li et al., 2017):

$$J = J_L - J_0 \left[exp\left(\frac{e(V+J\times R_S)}{AK_BT}\right) - 1 \right] - \frac{V+J\times R_S}{R_{SH}}$$

$$\tag{4}$$

Where:

J : The output voltage The produced current by SC The electric current induced from light : Ideality factor Α J_0 The reverse saturation current K_{b} : Boltzmann constant Е Т : Electron charge : Temperature Shunt resistances R_s Series resistances R_{sh}

3.5.1. Series Resistances (RS)

The main effect of the series resistances (R_S) is to reduce the FF, but extremely high values can also reduce the (J_{SC}), which means that it is not affected by the series resistance until it is very large. The (V_{OC}) is almost not influenced by the R_S because the total current flows through the solar cell and consequently the series resistance is zero (Honsberg & Bowden, 2019). In order to understand the series resistances effect on ideal device properties, the R_S value was changed between $0.5-50~\Omega.cm^2$ in SCAPS for all studied types. The obtained results are illustrated in Figure 8 and listed in Table 6. The simulation results clearly show that the increment in R_S value diminishes the PSC performance characteristics except V_{OC} .

Table 6. The simulated PSC devices performance parameters for Rs value 0.5 and 50 (Ω .cm²)

Simulated	PCE (%)	Voc (V)	-	Jsc (mA/c	m ²)	FF (%)	
Devices	$R_{S} = 0.5$	Rs = 50	$R_{S} = 0.5$	Rs = 50	Rs = 0.5	Rs = 50	$R_{S} = 0.5$	Rs = 50
	$(\Omega.cm^2)$	$(\Omega.cm^2)$	$(\Omega.cm^2)$	$(\Omega.cm^2)$	$(\Omega.cm^2)$	$(\Omega.cm^2)$	$(\Omega.cm^2)$	$(\Omega.cm^2)$
MAPbI3	24.51	5.50	1.13	1.13	25.25	21.40	86.07	22.77
MASnI3	21.53	3.98	0.87	0.87	29.96	16.80	83.03	27.32
FAPbI3	20.53	4.29	0.98	0.98	24.93	18.77	83.85	23.29
FASnI3	19.43	4.94	1.03	1.03	24.95	18.95	75.76	25.31
CsPbI3	16.06	4.59	0.98	0.98	18.92	17.98	86.46	26.00
CsGeI3	14.59	3.69	0.85	0.85	20.89	16.04	82.27	27.03
MAGeI3	12.54	6.22	1.18	1.18	12.67	12.66	84.11	41.72

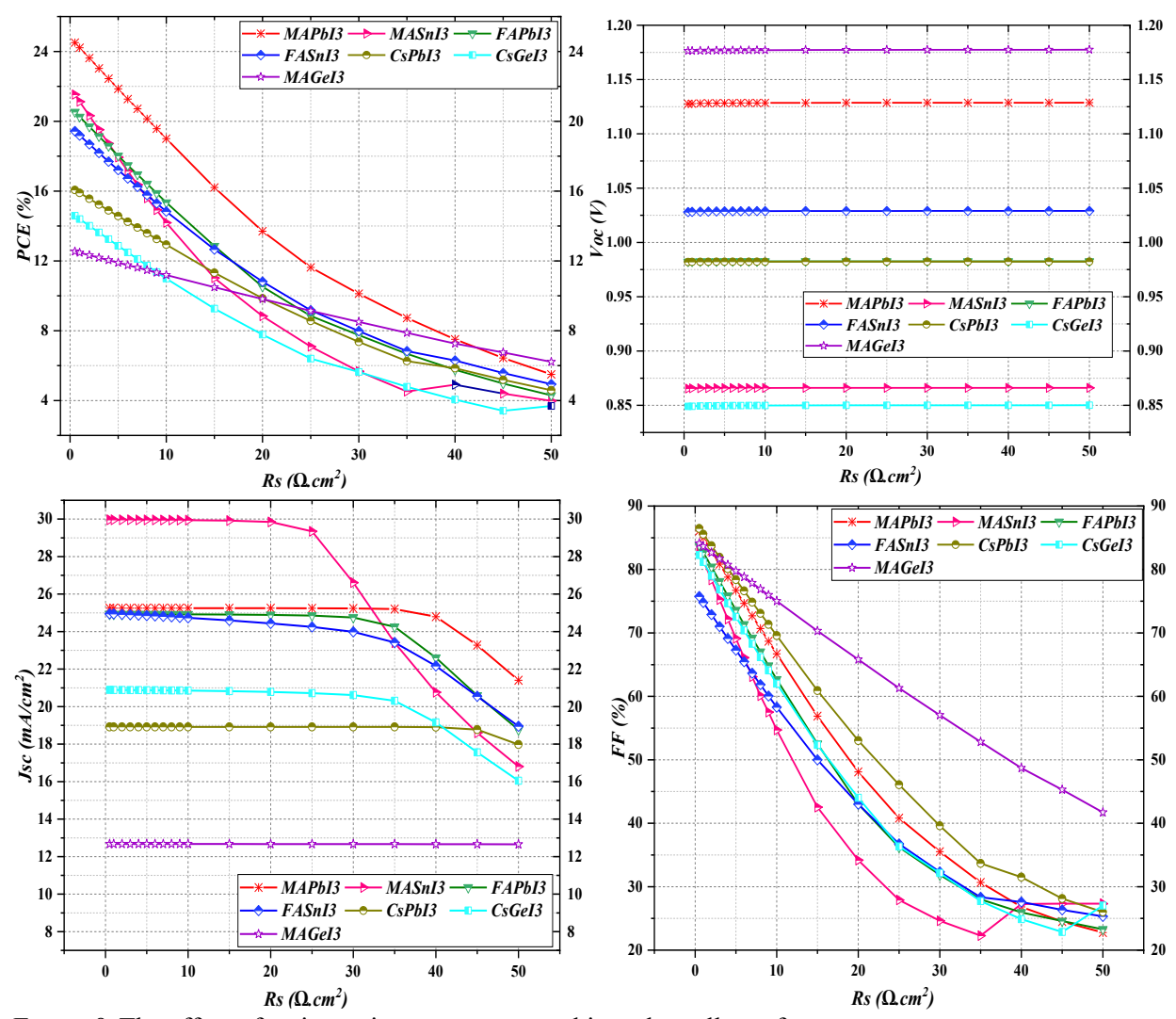


Figure 8. The effect of series resistances on perovskite solar cells performance

It can be concluded from the results that $MASnI_3$ -based is the most influenced device. By R_S increment, the J_{SC} drops quickly from 29.96 to just 16.80 mA/cm² and the PCE decreases from 21,53% to 3,98%. On the other hand, the least affected device was the MAGeI₃ based, where the J_{SC} is almost constant by increasing the R_S and the PCE drops from 12.54% to 6.22%.

3.5.2. Shunt Resistances (Rsh)

By providing an alternate path for the generated current, low R_{SH} causes losses in power in solar cells. This is accomplished by absorbing light, which reduces the amount of current passing through the solar cell junction, lowering the voltage produced by the solar cell. Because there is less light-induced current at low light levels, the effect of the shunt resistances is more severe (Honsberg & Bowden, 2019). In order to clarify the effect of shunt resistance, its value was changed between $50-1600~\Omega.cm^2$ for all devices and the simulation results were plotted in Figure 9.

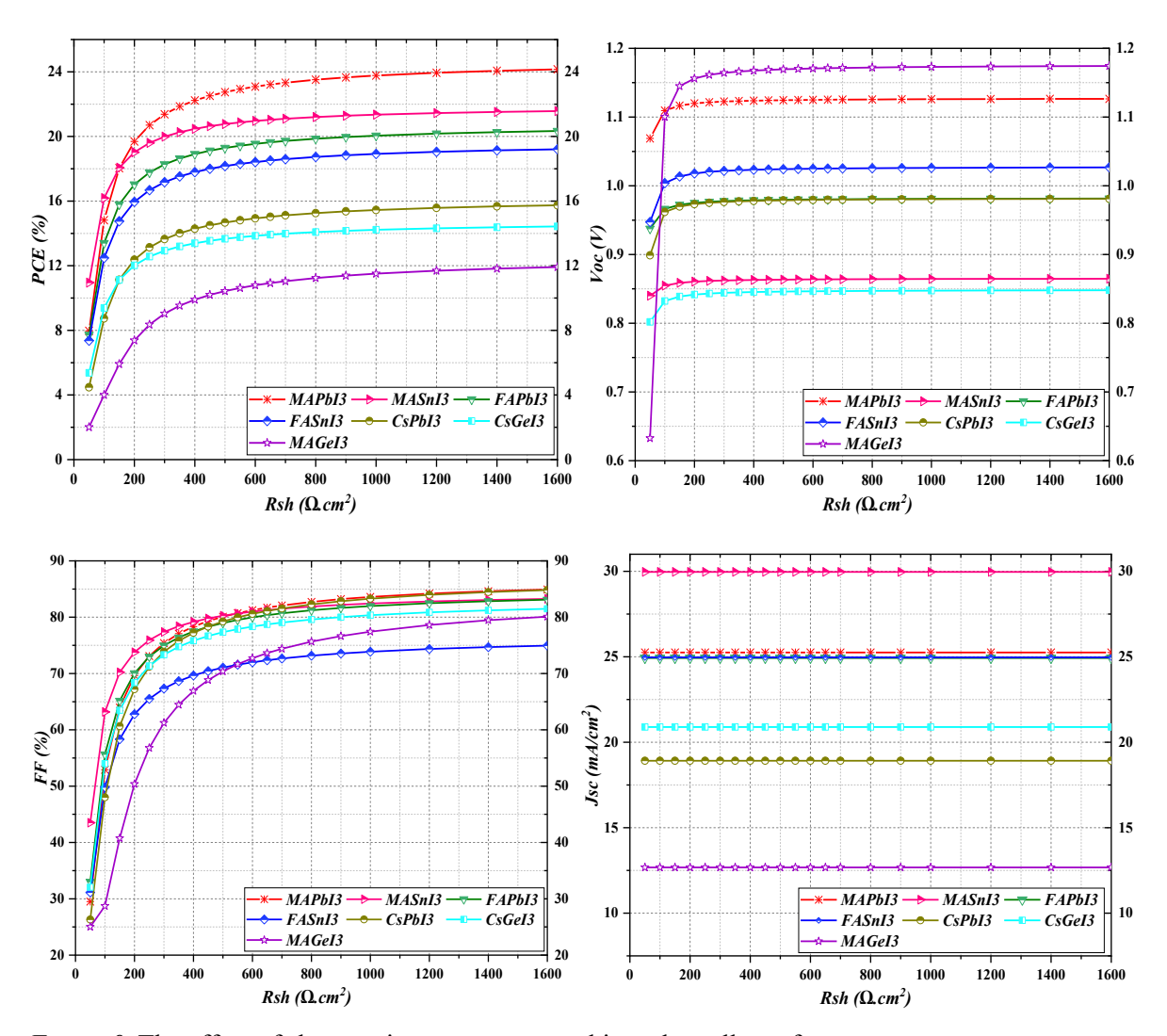


Figure 9. The effect of shunt resistances on perovskite solar cells performance

Similarly, in all studied devices, as the shunt resistances increase, the fill factor FF and PCE increase rapidly, while V_{OC} is only slightly affected by R_{SH} when its value is too low and J_{SC} is not affected at all (see Figure 9). Therefore, the enhancement in devices' efficiency can be explained by the FF increase.

3.6. The effect of the back contact metal

To find out whether another back contact can present a better or similar performance as gold being used, simulation for the selected devices was performed with nine possible back contacts. The potential back contacts and their work function are listed in Table 7. below and the obtained PSCs performance data plotted to Figure 10.

Table 7.

Work Function of Back Metal contacts (Behrouznejad et al., 2016; Deepthi Jayan & Sebastian, 2021; Raoui et al., 2019)

Back metal contact	Copper (Cu)	Silver (Ag)			Gold (Au)	U	Nickel (Ni)	Palladium (Pd)	Platinum (Pt)	Selenium (Se)
Work function (eV)	4.65	4.74	4.81	5	5.1	5.22	5.5	5.6	5.7	5.9

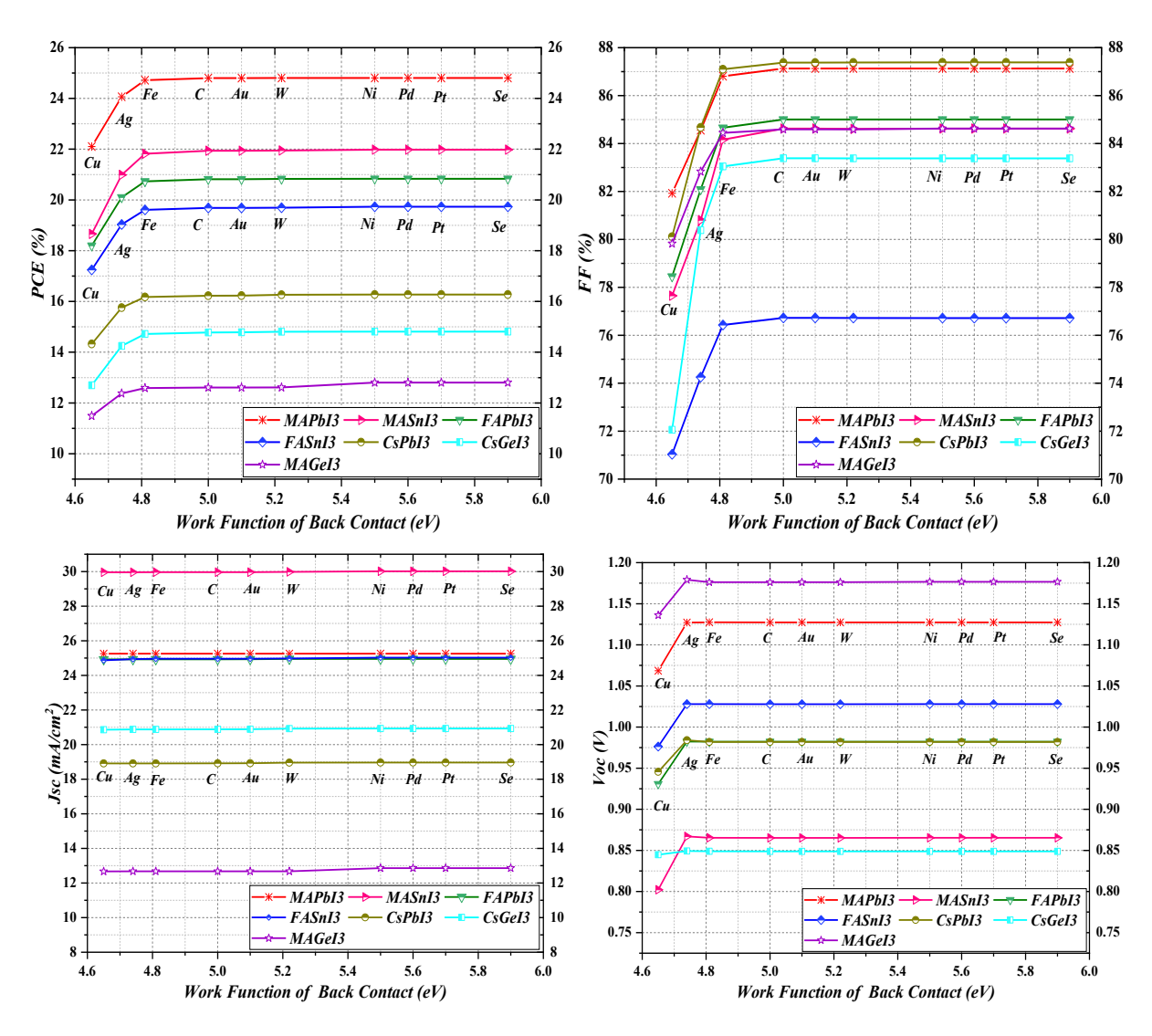


Figure 10. The effect of back contact on perovskite solar cells performance

Simulation results presented in Figure 10 illustrate that all devices performance increases correspondingly with the work function of the back contact until it reaches a negligible difference in PSC efficiency after (5 eV) for carbon, which means that carbon can be used instead of gold as a low-cost back metal contact.

3.7. CBO and VBO defining

Valence Band Offset (VBO) between the absorber and HTL and the Conduction Band Offset (CBO) between the absorber and ETL considerably affect the transport of carriers, and they have been accepted in three shapes: cliff shape, flat shape, and spike-like shape. Defining equations of CBO and VBO are given below by equation 5 and 6 respectively (Abnavi et al., 2021; Maram et al., 2021).

$$CBO = |\chi_{Absorber}| - |\chi_{HTL/ETL}|$$
 (5)

$$VBO = (|\chi_{Absorber}| + Eg_{Absorber}) - (|\chi_{HTL/ETL}| + Eg_{HTL/ETL})$$
 (6)

Where; χ refers to the electron affinity and E_g refers to the band gap.

According to these Equations, CBO and VBO values for perovskites have been calculated and listed in Table 8 and Table 9.

Table 8. *Calculation of conduction band offset values for each perovskite*

Perovskites	Electron affinity of	Electron affinity of	CBO (eV)
	Perovskite (eV)	ETL (eV)	
MAPbI ₃	3.9	4	- 0.1
$MASnI_3$	4.2	4	+ 0.2
FAPbI ₃	4.0	4	0
FASnI ₃	3.9	4	-0.1
CsPbI ₃	3.95	4	-0.05
MAGeI3	3.98	4	-0.02
CsGeI ₃	3.523	4	-0.477

Table 9. *Calculation of valance band offset values for each perovskite*

Perovskites	Perovskit Electron Affinity (eV)	Perovskit Band Gap (eV)	HTL Electron Affinity (eV)	HTL Band Gap (eV)	VBO
$MAPbI_3$	3.9	1.55	3.2	2.17	+ 0.08
$MASnI_3$	4.2	1.3	3.2	2.17	+0.13
$FAPbI_3$	4.0	1.51	3.2	2.17	+0.14
$FASnI_3$	3.9	1.41	3.2	2.17	-0.06
$CsPbI_3$	3.95	1.694	3.2	2.17	+0.0274
MAGeI3	3.98	1.9	3.2	2.17	+0.51
$CsGeI_3$	3.523	1.6	3.2	2.17	-0.247

When the energy difference is zero, as in the case of the CBO of FAPbI3 (see Table 8.), then the shape is nearly flat, which means that there is no band offset and consequently no barrier for the transport of charge carriers (generated electrons or holes). The band alignment of the absorber/ETL (absorber/HTL) exhibits a spike-like appearance for tiny positive (negative) CBO (VBO) values, preventing recombination at the interface. When CBO (VBO) is negative (positive), the absorber/ETL (absorber/HTL) band alignment is cliff-like, facilitating increased and faster recombination at the interface (Abnavi et al., 2021; Maram et al., 2021).

A significant reduction in J_{SC} and FF is associated with large positive (negative) CBO (VBO) values. This reduction is owing to the formation of a strong barrier against electrons (holes) that is generated by light (Abnavi et al., 2021; Yan et al., 2014).

4. Conclusion

The presented simulation study has been done via SCAPS-1D software for three different structures of lead-based perovskites, MAPbI₃, FAPbI₃ and CsPbI₃, and four lead-free perovskites, MASnI₃, FASnI₃, CsGeI₃, and MAGeI₃ as absorbing layer with TiO₂ and Cu₂O as ETL and HTL respectively, with the device configuration of FTO/TiO₂/perovskite (absorber layer) /Cu₂O/Au. The influences of different factors on the performance of perovskite solar cells have been studied, including the thickness and the total defect density of the absorber layer, the parasitic resistances, and the operating temperature in order to optimize the device configuration and improve the PSC efficiency. All perovskite types exhibit nearly identical effects on the studied factors.

Acknowledgement

We would like to thank Dr. Marc Burgelman, Department of Electronics and Information Systems (ELIS), University of Gent, Belgium, for providing the SCAPS-1D simulation software.

This research did not receive any specific grant from funding agencies in the public, commercial, or not-for-profit sectors.

References

- Abdelaziz, S., Zekry, A., Shaker, A., & Abouelatta, M. (2020). Investigating the performance of formamidinium tin-based perovskite solar cell by SCAPS device simulation. *Optical Materials*, 101, 109738. https://doi.org/10.1016/J.OPTMAT.2020.109738
- Abnavi, H., Maram, D. K., & Abnavi, A. (2021). Performance analysis of several electron/hole transport layers in thin film MAPbI3-based perovskite solar cells: A simulation study. *Optical Materials*, *118*, 111258. https://doi.org/10.1016/j.optmat.2021.111258
- Behrouznejad, F., Shahbazi, S., Taghavinia, N., Wu, H.-P., & Wei-Guang Diau, E. (2016). A study on utilizing different metals as the back contact of CH3NH3PbI3 perovskite solar cells. *J. Mater. Chem. A*, 4(35), 13488–13498. https://doi.org/10.1039/C6TA05938D
- Burgelman, M., Decock, K., Niemegeers, A., Verschraegen, J., & Degrave, S. (2021). SCAPS Manual. *University of Gent, february*.
- Burgelman, M., Nollet, P., & Degrave, S. (2000). Modelling polycrystalline semiconductor solar cells. *Thin Solid Films*, 361–362, 527–532. https://doi.org/10.1016/S0040-6090(99)00825-1
- Chakraborty, K., Choudhury, M. G., & Paul, S. (2019). Numerical study of Cs2TiX6 (X = Br-, I-, F- and Cl-) based perovskite solar cell using SCAPS-1D device simulation. *Solar Energy*, 194, 886–892. https://doi.org/10.1016/j.solener.2019.11.005
- Chen, L. C., Tseng, Z. L., & Huang, J. K. (2016). A study of inverted-type perovskite solar cells with various composition ratios of (FAPBI3)1–x(MAPbBr3)x. *Nanomaterials*, 6(10), 1–8. https://doi.org/10.3390/nano6100183
- Courtier, N. E., Cave, J. M., Walker, A. B., Richardson, G., & Foster, J. M. (2019). IonMonger: a free and fast planar perovskite solar cell simulator with coupled ion vacancy and charge carrier dynamics. *Journal of Computational Electronics*, *18*(4), 1435–1449. https://doi.org/10.1007/s10825-019-01396-2
- Courtier, Nicola E., Cave, J. M., Foster, J. M., Walker, A. B., & Richardson, G. (2019). How transport layer properties affect perovskite solar cell performance: Insights from a coupled charge transport/ion migration model. *Energy and Environmental Science*, *12*(1), 396–409. https://doi.org/10.1039/c8ee01576g
- Deepthi Jayan, K., & Sebastian, V. (2021). Comprehensive device modelling and performance analysis of MASnI3 based perovskite solar cells with diverse ETM, HTM and back metal contacts. *Solar Energy*, *217*, 40–48. https://doi.org/10.1016/j.solener.2021.01.058
- Gélvez-Rueda, M. C., Renaud, N., & Grozema, F. C. (2017). Temperature Dependent Charge Carrier Dynamics in Formamidinium Lead Iodide Perovskite. *Journal of Physical Chemistry C*, 121(42), 23392–23397. https://doi.org/10.1021/acs.jpcc.7b09303
- Honsberg, C., & Bowden, S. (2019). *Photovoltaics Education Website*. Photovoltaics Education Website. https://www.pveducation.org/pvcdrom

- Houimi, A., Gezgin, S. Y., Mercimek, B., & Kılıç, H. Ş. (2021). Numerical analysis of CZTS/n-Si solar cells using SCAPS-1D. A comparative study between experimental and calculated outputs. *Optical Materials*, *121*, 111544. https://doi.org/10.1016/J.OPTMAT.2021.111544
- Jayan K, D., Sebastian, V., & Kurian, J. (2021). Simulation and optimization studies on CsPbI3 based inorganic perovskite solar cells. *Solar Energy*, 221, 99–108. https://doi.org/10.1016/J.SOLENER.2021.04.030
- Kanoun, A. A., Kanoun, M. B., Merad, A. E., & Goumri-Said, S. (2019). Toward development of high-performance perovskite solar cells based on CH3NH3GeI3 using computational approach. *Solar Energy*, 182, 237–244. https://doi.org/10.1016/j.solener.2019.02.041
- Karimi, E., & Ghorashi, S. M. B. (2017). Investigation of the influence of different hole-transporting materials on the performance of perovskite solar cells. *Optik*, *130*, 650–658. https://doi.org/10.1016/J.IJLEO.2016.10.122
- Karthick, S., Velumani, S., & Bouclé, J. (2020). Experimental and SCAPS simulated formamidinium perovskite solar cells: A comparison of device performance. *Solar Energy*, 205, 349–357. https://doi.org/10.1016/j.solener.2020.05.041
- Kumar, M., Kumar, A., Raj, A., Sati, P. C., Sahni, M., & Anshul, A. (2022). Organic-inorganic perovskite-based solar cell designs for high conversion efficiency: A comparative study by SCAPS simulation. *Materials Today: Proceedings*, 49, 3081–3087. https://doi.org/10.1016/j.matpr.2020.11.035
- Kumar, M., Raj, A., Kumar, A., & Anshul, A. (2020). An optimized lead-free formamidinium Sn-based perovskite solar cell design for high power conversion efficiency by SCAPS simulation. *Optical Materials*, *108*, 110213. https://doi.org/10.1016/J.OPTMAT.2020.110213
- Lenka, T. R., Soibam, A. C., Dey, K., Maung, T., & Lin, F. (2020). Numerical analysis of high-efficiency lead-free perovskite solar cell with NiO as hole transport material and PCBM as electron transport material. *CSI Transactions on ICT*, 8(2), 111–116. https://doi.org/10.1007/s40012-020-00291-7
- Li, Y., Ding, B., Chu, Q. Q., Yang, G. J., Wang, M., Li, C. X., & Li, C. J. (2017). Ultra-high open-circuit voltage of perovskite solar cells induced by nucleation thermodynamics on rough substrates. *Scientific Reports*, 7(March), 1–10. https://doi.org/10.1038/srep46141
- Liu, D., Gangishetty, M. K., & Kelly, T. L. (2014). Effect of CH3NH3PbI3 thickness on device efficiency in planar heterojunction perovskite solar cells. *J. Mater. Chem. A*, 2(46), 19873–19881. https://doi.org/10.1039/C4TA02637C
- Maram, D. K., Haghighi, M., Shekoofa, O., Habibiyan, H., & Ghafoorifard, H. (2021). A modeling study on utilizing ultra-thin inorganic HTLs in inverted p—n homojunction perovskite solar cells. *Solar Energy*, *213*, 1–12. https://doi.org/10.1016/J.SOLENER.2020.11.009
- Minemoto, T., & Murata, M. (2014). Impact of work function of back contact of perovskite solar cells without hole transport material analyzed by device simulation. *Current Applied Physics*, *14*(11), 1428–1433. https://doi.org/10.1016/j.cap.2014.08.002
- Nalianya, M. A., Awino, C., Barasa, H., Odari, V., Gaitho, F., Omogo, B., & Mageto, M. (2021). Numerical study of lead free CsSn0.5Ge0.5I3 perovskite solar cell by SCAPS-1D. *Optik*, 248(May), 168060. https://doi.org/10.1016/j.ijleo.2021.168060
- NREL. (2022). Best Research-Cell Efficiency Chart. https://www.nrel.gov/pv/cell-

efficiency.html

- Patel, P. K. (2021). Device simulation of highly efficient eco-friendly CH3NH3SnI3 perovskite solar cell. *Scientific Reports*, 11(1), 3082. https://doi.org/10.1038/s41598-021-82817-w
- Raj, A., Kumar, M., Singh, P. K., Chandra Singh, R., Bherwani, H., Gupta, A., & Anshul, A. (2021). A computational approach to investigate the suiTable ETL for lead-free CsGeI3based perovskite solar cell. *Materials Today: Proceedings*, 47, 1564–1569. https://doi.org/10.1016/j.matpr.2021.03.610
- Raoui, Y., Ez-Zahraouy, H., Tahiri, N., El Bounagui, O., Ahmad, S., & Kazim, S. (2019). Performance analysis of MAPbI3 based perovskite solar cells employing diverse charge selective contacts: Simulation study. *Solar Energy*, *193*, 948–955. https://doi.org/10.1016/J.SOLENER.2019.10.009
- Raza, E., Ahmad, Z., Aziz, F., Asif, M., Ahmed, A., Riaz, K., Bhadra, J., & Al-Thani, N. J. (2021). Numerical simulation analysis towards the effect of charge transport layers electrical properties on cesium based ternary cation perovskite solar cells performance. *Solar Energy*, 225, 842–850. https://doi.org/10.1016/j.solener.2021.08.008
- Sarker, S., Islam, M. T., Rauf, A., Al Jame, H., Jani, M. R., Ahsan, S., Islam, M. S., Nishat, S. S., Shorowordi, K. M., & Ahmed, S. (2021). A SCAPS simulation investigation of nontoxic MAGeI3-on-Si tandem solar device utilizing monolithically integrated (2-T) and mechanically stacked (4-T) configurations. *Solar Energy*, 225(May), 471–485. https://doi.org/10.1016/j.solener.2021.07.057
- Singh, A. K., Srivastava, S., Mahapatra, A., Baral, J. K., & Pradhan, B. (2021). Performance optimization of lead free-MASnI3 based solar cell with 27% efficiency by numerical simulation. *Optical Materials*, *117*, 111193. https://doi.org/10.1016/j.optmat.2021.111193
- Singh, R., Giri, A., Pal, M., Thiyagarajan, K., Kwak, J., Lee, J. J., Jeong, U., & Cho, K. (2019). Perovskite solar cells with an MoS2 electron transport layer. *Journal of Materials Chemistry A*, 7(12), 7151–7158. https://doi.org/10.1039/c8ta12254g
- Slami, A., Bouchaour, M., & Merad, L. (2020). Comparative study of modeling of Perovskite solar cell with different HTM layers. *International Journal of Materials*, 7, 1–5. https://doi.org/10.46300/91018.2020.7.1
- Tang, H., He, S., & Peng, C. (2017). NANO REVIEW Open Access A Short Progress Report on High-Efficiency Perovskite Solar Cells. *Nanoscale Research Letters*, 12, 410. https://doi.org/10.1186/s11671-017-2187-5
- Tao, S., Schmidt, I., Brocks, G., Jiang, J., Tranca, I., Meerholz, K., & Olthof, S. (2019). Absolute energy level positions in tin- and lead-based halide perovskites. *Nature Communications*, 10(1), 2560. https://doi.org/10.1038/s41467-019-10468-7
- Tara, A., Bharti, V., Sharma, S., & Gupta, R. (2021). Device simulation of FASnI3 based perovskite solar cell with Zn(O0.3, S0.7) as electron transport layer using SCAPS-1D. *Optical Materials*, 119, 111362. https://doi.org/10.1016/J.OPTMAT.2021.111362
- Tonui, P., Oseni, S. O., Sharma, G., Yan, Q., & Tessema Mola, G. (2018). Perovskites photovoltaic solar cells: An overview of current status. *Renewable and Sustainable Energy Reviews*, 91, 1025–1044. https://doi.org/10.1016/J.RSER.2018.04.069
- Yan, C., Liu, F., Song, N., Ng, B. K., Stride, J. A., Tadich, A., & Hao, X. (2014). Band alignments of different buffer layers (CdS, Zn(O,S), and In 2 S 3) on Cu 2 ZnSnS 4. *Applied Physics Letters*, 104(17), 173901. https://doi.org/10.1063/1.4873715

Zhao, Y. Q., Liu, B., Yu, Z. L., Ma, J. M., Wan, Q., He, P. Bin, & Cai, M. Q. (2017). Strong ferroelectric polarization of CH3NH3GeI3 with high-absorption and mobility transport anisotropy: Theoretical study. *Journal of Materials Chemistry C*, 5(22), 5356–5364. https://doi.org/10.1039/c7tc01166k